Journal of Mathematical Control Science and Applications (JMCSA)
Vol. 4 No. 1 (January-June, 2018), ISSN : 0974-0570

Nonlinear Dynamic Modeling and Speed Control for a Cruise Missile Turbofan Engine

Tain-Sou Tsay*

Abstract: In this brief paper, nonlinear dynamic models and a speed governor with temperature suppression are proposed for a cruise missile turbofan engine. The dynamic models give mathematical description of the physical system. Engine temperature estimator with measurable signals is used for temperature suppressing control and providing good system integrity. From the real testing and simulation results of the controlled system, one can see that proposed dynamic models give good agreement with the real system and the nonlinear speed governor makes the controlled system have good performance and less engine temperature increment than that of the linear speed governor.

Keywords: Nonlinear Engine Modeling, Engine Speed Control, Nonlinear Controller

1. INTRODUCTION

The turbofan engine considered in this brief paper is used in a long-range unmanned flight vehicle for digital scene sensing. Constant flight speed with respect to ground is generally required for large area image sensing systems [1-3]. Since the weight of the vehicle is decreasing from fuel consumption and large maneuvers. The engine speed feedback control loop for propelling force adjustment is need. The thermal transfer of the engine, which is packed in the compact vehicle, must be concerned also for long time operation. The higher engine speed obtained, the higher engine temperature will be. The higher speed is corresponding to greater volume of fuel filled in. This implies that unexpected temperature increment due to unexpected extra volume of fuel to the engine, and good engine speed control performance is generally required for preventing unexpected fuel filled in.

The relationships between engine speed, engine temperature, fuel supply rate and fuel throttle angle determine characteristics of the considered system. They must be modeled for analyzing and designing the speed feedback control system. Taiwo [4] proposed a 24th-order plant which consists of an F100 turbofan engine and throttle actuators; Mahil and Bommaraja [5] proposed a sixteenth-order linear dynamical model and reduced it to be fourth-order model for analyses and controller designs. There are several other researching efforts [6-9] for modeling the turbofan engine. Although they provided good descriptions for the turbofan engine, but they need complicated identification process in frequency domain or time domain. In the literature, two dynamic models with a simple first-order model are proposed. They are derived from measurement datum of steady-state values of fuel supply rate, engine temperature and engine speed for a specified value of fuel throttle angle. The modeling process is much simpler than those of stated in Refs. [4-9].

There are several recent researching work for engine speed controls including neural network by Kulkami [10], sliding mode by Tournes and Puleston [11,12], LQG/LTR by Kwitegetse [13] and robust control by Merrill [14]. Generally speaking, the latter control strategies may still lead to implementation difficulties,

* Department of Aeronautical Engineering, National Formosa University, 64, Wen Hua Road, Huwei, Yunlin, 632, Taiwan.
E-mail: tstsay@nfu.edu.tw

compared to linear or simple nonlinear controllers; e.g., nonlinear PI controller. Integration gain for exact speed command tracking is generally required for vehicle speed control. But the windup problem must be concerned for saturation or limitation characteristics of the considered system (e.g., throttle angle). Kapoor et al. [15] and Frederick et al. [16] discussed anti-windup synthesis formulation schemes for integrator gains after nominal H_∞ controller found. The H_∞ controller is a perfect design, but the anti-windup syntheses degraded the performances of the overall system with nominal H_∞ controller. In this literature, PI controller with a new anti-windup scheme is proposed. It improves performance significantly from the linear system design.

In following sections, the larger and small models of the overall system for analyses, designs, and simulations are evaluated first, and then frequency responses analyses are used to find desired speed governor, and finally overall system simulation verifications are used to find suitable command rate limitations and saturation level of the output of the speed governor. The design results are verified by real testing datum also. Simulation and real testing results will show that the proposed models give excellent description for the real system and proposed compensations make the controlled system give good performance and lower unexpected temperature increment.

2. SYSTEM DESCRIPTIONS

The overall system is shown in Fig.1; in which the block $Q(s, \alpha)$ represents dynamics of the fuel supply device; the block $E(s, Q_F)$ represents dynamics of the engine; the block $A(s)$ represents the fuel throttle angle servo actuating system. α_0 and α_1 represent the lower and upper limitations of the throttle angle. The block $T(Q_F, N_G)$ represents the engine temperature T_G estimator. It replaces the thermal coupler for high integrity. Inputs of the temperature estimator are two measurable and realizable variables. They are the fuel supply rate Q_F and the engine speed N_G. The outer loop is used for engine speed regulating which is consisted of speed governor $G_o(s)$, feedback phase compensation $H_o(s)$, and speed feedback signal noise filter $F_o(s)$. The controller $G_o(s)$ is a PI controller with anti-windup [17,18]. The inner loop will be activated when the engine temperature estimation $T_{G,est}$ is greater than suppressing temperature T_o . It is consisted of noise filter $F_i(s)$, T_o detector, phase compensation $H_i(s)$, and rate limiter $G_i(s)$. Lower throttle angle command α_C will be manipulated when $T_{G,est}$ is greater than T_o. This implies that less fuel will be filled into the engine. The controller $G_i(s)$ is a rate limiter which gives different increasing and decreasing rate limitations for speeding up and down. Positive limitation is used for decreasing temperature increment and negative limitation is used for preventing burn-off.

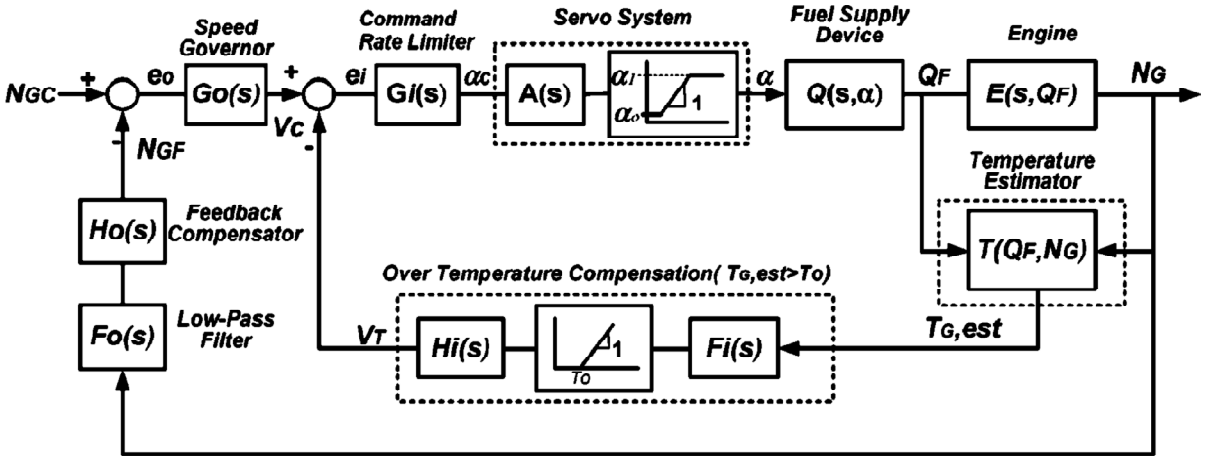

Figure 1: Speed Control Configuration of the Turbofan Engine

Now, consider the steady-state values of the fuel throttle angle α_{SS}, the fuel supply rate $Q_{F,SS}$, the engine speed $N_{G,SS}$ and the engine temperature $T_{G,SS}$. Fig. 2(a) shows measured datum (dot) for $Q_{F,SS}$ versus α_{SS}; Fig. 2(b) shows measured datum (dot) for $N_{G,SS}$ versus $Q_{F,SS}$; Fig. 2(c) shows measured datum(dot) for $T_{G,SS}$ versus $N_{G,SS}$. The notations $\bar{Q}_F(\alpha)$, $\bar{N}_G(Q_F)$ and $\bar{T}_G(N_G)$ shown in Figs. 2(a), 2(b) and 2(c) are curve fitting representations from measured datum. Since the engine has unique equilibrium state, the relationship between $T_{G,SS}$, $N_{G,SS}$ and $Q_{F,SS}$ is unique for a specified value of α_{SS}. $T_{G,SS}$ and $Q_{F,SS}$ will be used alternatively in mathematical formulations. Fig. 2(b) shows that the engine speed $N_{G,SS}$ is saturated at 35000RPM for larger value of $Q_{F,SS}$, (>550 LPH), and Fig. 2(a) shows that the fuel supply rate $Q_{F,SS}$ is saturated at 700 LPH for larger values of the throttle angle α_{SS} (>100°). Figs. 2(a), 2(b) and 2(c) show all characteristic curves are nonlinear and the engine is designed for the operating speed below 35000RPM and the engine temperature below 700°C. The value of T_o shown in Fig. 1 must be greater than or equal to that of $T_{G,SS}$; which is corresponding to the desired maximal operating speed $N_{G,SS}$.

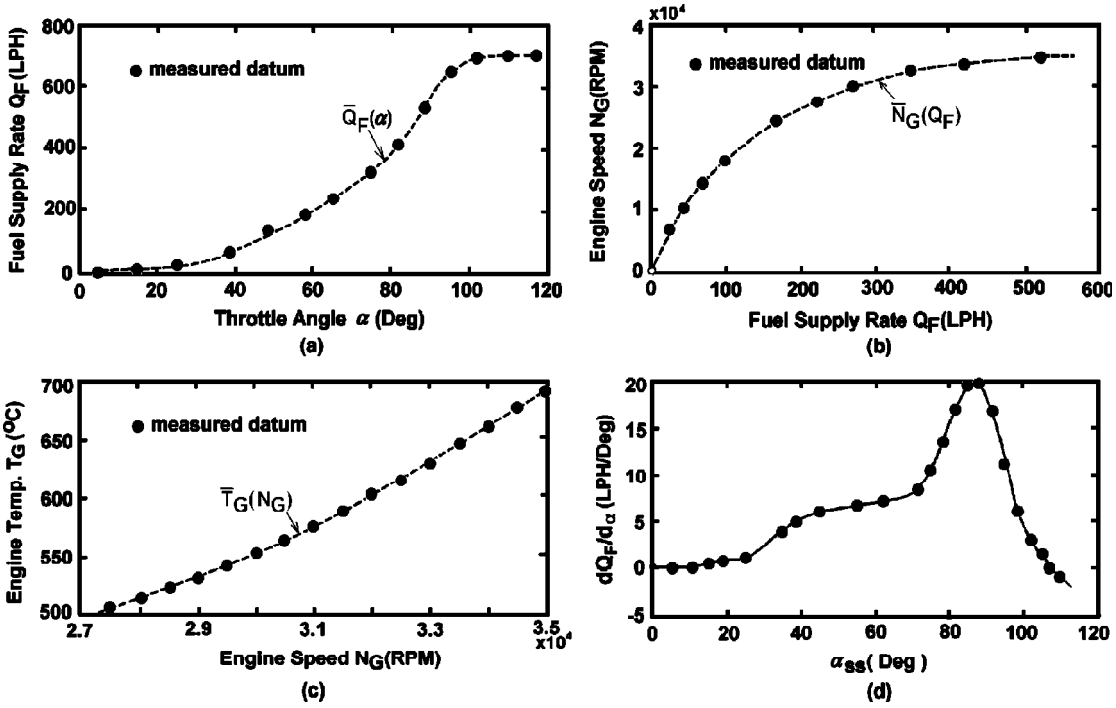

Figure 2: Measured Datum (a) $Q_{F,SS}$, vs. α_{SS}, (b) $N_{G,SS}$, vs. $Q_{F,SS}$, (c) $T_{G,SS}$, vs. $N_{G,SS}$, (d) $dQ_F(\alpha)/d\alpha|_{\alpha=\alpha_{SS}}$ vs. α_{SS} .

3. DYNAMIC MODELS OF THE PLANT AND TEMPERATURE ESTIMATOR

The dynamic models to be evaluated are $Q(s, \alpha)$, $E(s, Q_F)$ and $T(Q_F, N_G)$. They are shown in Fig.1. Consider the deviation of Q_F with respect to α around steady-state condition α_{SS}; it is in the form of

$$\Delta Q_F = \left.\frac{dQ_F(\alpha)}{d\alpha}\right|_{\alpha=\alpha_{SS}} \times \Delta\alpha = \left.\frac{dQ_F(\alpha)}{d\alpha}\right|_{\alpha=\alpha_{SS}} \times (\alpha - \alpha_{SS}) \tag{1}$$

and

$$\Delta Q_F \cong \left.\frac{dQ_F(\alpha)}{d\alpha}\right|_{\alpha=\alpha_{SS}} \times \left[\alpha - \bar{Q}_F^{-1}(x)\Big|_{x=Q_{F,SS}}\right] \tag{2}$$

where $\alpha_{SS} \equiv \bar{Q}_F^{-1}(x)\Big|_{x=Q_{F,SS}}$ represents solution x of $Q_{F,SS} = \bar{Q}_F(x)$, and α_{SS}, and $dQ_F(\alpha)/d\alpha|_{a=a_{SS}}$ is derived from $Q_F = \bar{Q}_F(\alpha)$ shown in Fig. 2(a). The values of $dQ_F(\alpha)/d\alpha|_{a=a_{SS}}$ versus α_{SS} are illustrated in Fig. 2(d). Since the fuel supply device is a low-pass system, the variation of Q_F is much slower than that of α, the term $\bar{Q}_F^{-1}(x)\Big|_{x=Q_{F,SS}}$ of Eq.(2) can be approximated by $\bar{Q}_F^{-1}(x)\Big|_{x=Q_F}$; i.e.,

$$\alpha_F \equiv \bar{Q}_F^{-1}(x)\Big|_{x=Q_F} \approx \bar{Q}_F^{-1}(x)\Big|_{x=Q_{F,SS}} = \alpha_{SS} \tag{3}$$

and Eq.(2) becomes

$$\Delta Q_F \cong \frac{dQ_F(\alpha)}{d\alpha}\Big|_{\alpha=\alpha_F} \times \left[\alpha - \bar{Q}_F^{-1}(x)\Big|_{x=Q_F}\right] \tag{4}$$

Then, the derivative of the Q_F with respect to time can be formulated as in the form of

$$\dot{Q}_F = \Delta Q_F / \tau_V \tag{5}$$

where τ_v represents the time constant of the fuel supply dynamics. The block diagram of the fuel supply dynamic with Equations (3) to (5) is shown in the upper-left part of Fig. 3. Similar to derivations of the fuel flowing dynamic $Q(s, \alpha)$, the engine dynamic $E(s, Q_F)$ at a steady-state conditions ($N_{G,SS}$ $Q_{F,SS}$) is formulated and discussed as below:

$$\Delta N_G = \frac{dN_G(Q_F)}{dQ_F}\Big|_{Q_F=Q_{F,SS}} \times \Delta Q_F = \frac{dN_G(Q_F)}{dQ_F}\Big|_{Q_F=Q_{F,SS}} \times (Q_F - Q_{F,SS}) \tag{6}$$

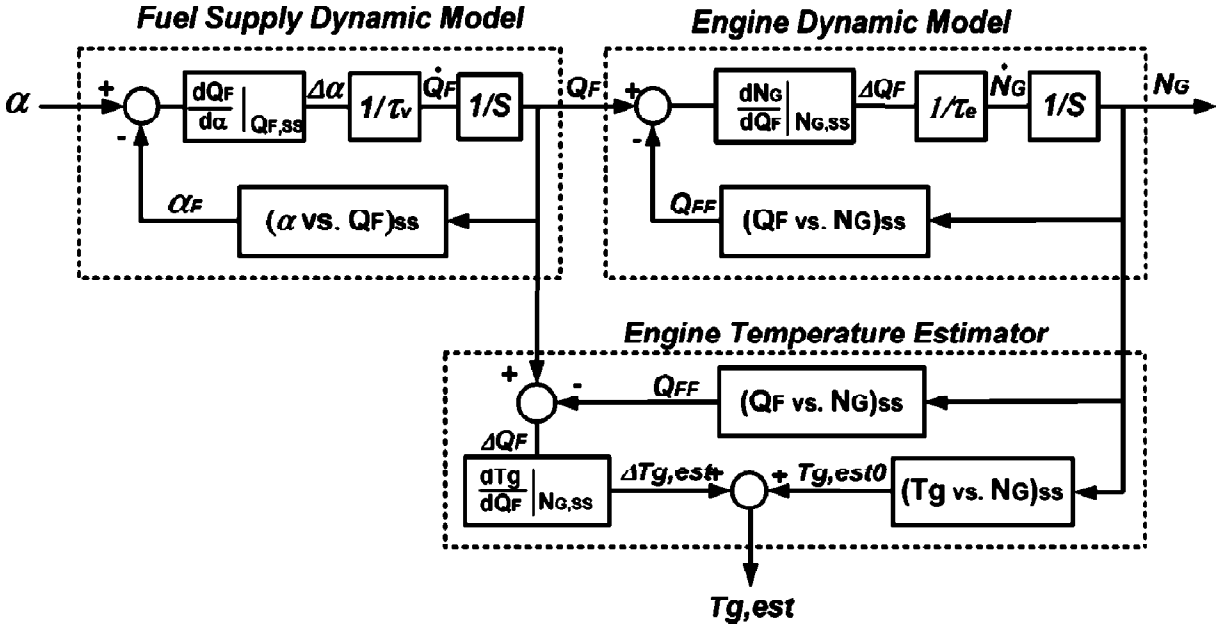

Figure 3: Dynamic Model of the Turbofan Engine with Temperature Estimator.

and

$$\Delta N_G = \left.\frac{dN_G(Q_F)}{dQ_F}\right|_{Q_F=Q_{F,SS}} \times \left[Q_F - \bar{N}_G^{-1}(y)\Big|_{y=N_{G,SS}} \right] \tag{7}$$

where $Q_{F,SS} \equiv \bar{N}_G^{-1}(y)\Big|_{y=N_{G,SS}}$ and $d_{NG}(Q_F)/dQ_F|_{Q_F=Q_{F,SS}}$ are derived from the relationship $N_G = \bar{N}_G(Q_F)$ shown in Fig. 2(b). Eq. (7) can be rewritten as

$$\Delta N_G = \left.\frac{dN_G(Q_F)}{dQ_F}\right|_{Q_F=Q_{FF}} \times \left[Q_F - \bar{N}_G^{-1}(y)\Big|_{y=N_G} \right] \tag{8}$$

where $\bar{N}_G^{-1}(y)\Big|_{y=N_{G,SS}}$ of Eq. (7) is approximated by $\bar{N}_G^{-1}(y)\Big|_{y=N_G}$ for the variation of N_G is much slower than that of Q_F also; i.e.,

$$Q_{FF} \equiv \bar{N}_G^{-1}(y)\Big|_{y=N_G} \cong \bar{N}_G^{-1}(y)\Big|_{y=N_{G,SS}} = Q_{F,SS} \tag{9}$$

and the derivative of N_G with respect to time is formulated as in the form of

$$\dot{N}_G = \Delta N_G / \tau_e \tag{10}$$

where τ_e represents the time constant of the engine dynamics. The block diagram of the engine dynamic described by Eqs.(8) to (10) is shown in the upper-right part of Fig. 3 also. It will be seen that first order models given by Eqs. (5) and (10) are enough for the considered plant.

Now, consider the temperature estimator of the engine. Taking the Taylor expansion of the engine rear temperature T_G with respect to $T_{G,SS}$, one has

$$T_G = \bar{T}_G(N_{G,SS}) + \left.\frac{dT_G(N_G)}{dN_G}\right|_{N_G=N_G,ss} \times (N_G - N_{G,SS}) + \left.\frac{dT_G(N_G)}{dQ_F}\right|_{N_G=N_G,ss} \times (Q_F - Q_{F,SS}) + high\ \ order\ \ terms \tag{11}$$

and

$$T_G = \bar{T}_G(N_{G,SS}) + \left.\frac{dT_G(N_G)}{dN_G}\right|_{N_G=N_G,ss} \times (N_G - N_{G,SS})$$

$$+ \left.\frac{dT_G(N_G)}{dN_G}\right|_{N_G=N_G,ss} \left.\frac{dN_G(Q_F)}{dQ_F}\right|_{Q_F=Q_{F,SS}} \times (Q_F - Q_{F,SS}) + high\ order\ terms \tag{12}$$

where $dN_G(Q_F)/dQ_F|_{(Q_F=Q_{F,SS}}$ and $dT_G(N_G)/dN_G|_{N_G=N_G,SS}$ are derived from the steady-state relationships between

$N_{G,SS}$ versus $Q_{F,SS}$, and $T_{G,SS}$ versus $N_{G,SS}$ give in Fig. 2(b) and Fig. 2(c); respectively. Neglecting high order terms of Eq. (12), one has

$$T_G \approx \overline{T}_G(N_{G,SS}) + \left.\frac{dT_G(N_G)}{dN_G}\right|_{N_G=N_{G,ss}} \times (N_G - N_{G,SS})$$

$$+ \left.\frac{dT_G(N_G)}{dN_G}\right|_{N_G=N_{G,ss}} \times \left.\frac{dN_G(Q_F)}{dQ_F}\right|_{Q_F=Q_{F,SS}} \times (Q_F - Q_{F,SS}) \tag{13}$$

Since the variation of engine speed N_G is much slower than that of Q_F, Eq. (13) can be further modified for temperature estimation. It is in the form of

$$T_{G,est} \equiv \overline{T}_G(N_G) + \left.\frac{dT_G(N_G)}{dN_G}\right|_{N_G,SS=N_G} \left.\frac{dN_G(Q_F)}{dQ_F}\right|_{Q_{F,SS}=Q_F} \times (Q_F - Q_{F,SS}) \tag{14}$$

and

$$T_{G,est} \equiv \overline{T}_G(N_G) + \left.\frac{dT_G(N_G)}{dN_G}\right|_{N_G,SS=N_G} \left.\frac{dN_G(Q_F)}{dQ_F}\right|_{Q_{F,SS}=Q_F} \times \left[Q_F - \overline{N}_{G,SS}^{-1}(y)\big|_{y=N_G} \right] \tag{15}$$

Eq. (15) gives that temperature estimator is function of Q_F and N_G. Note that the derivative terms and state-state values of Eqs. (1)-(15) are derived from the measured data shown in Figs. 2(a), 2(b) and 2(c). Fig. 3 is the dynamic model for digital simulations. The values of time constants τ_v and τ_e are evaluated from the step responses of the physical system for specified value of α. The model system dynamics is represented by Eqs.(4), (5), (8), (10), (15) with measured datum given Figs. 2(a)-2(c). Fig. 3 represents the connections.

The dynamic models shown in Fig. 3 will be become to small signal models after due to terms $\overline{N}_G^{-1}(y)\big|_{y=N_G}$, $\overline{Q}_F^{-1}(x)\big|_{x=Q_F}$ and $\overline{T}_G(N_{G,SS})$ replaced by derivative terms $[dN_G(Q_F)/dQ_F\big|_{Q_F=Q_{F,SS}}]^{-1} = dQ_F(\alpha)/d\alpha|_{\alpha=\alpha_{SS}}]^{-1}$ and $dT_{G,S}(N_G)/dN_G|_{N_G=N_{G,ss}}$; respectively. Fig. 4 shows the small signal model derived from Fig.3. Taking the frequency

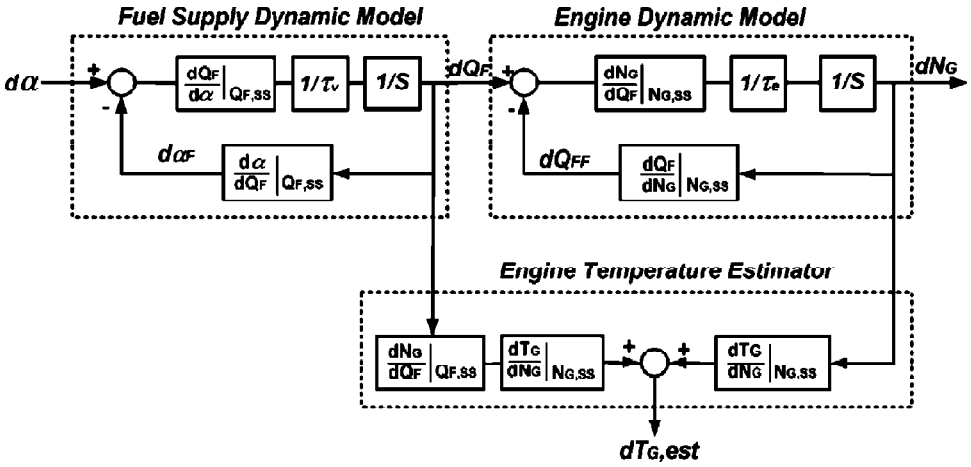

Figure 4: Small Signal Model of the Turbo Engine with Temperature Estimator

responses of the fuel supply device and the engine with τ_v and τ_e found in step responses. They are 0.53 and 0.035; respectively. Fig. 5(a) shows frequency responses of $Q(s, \alpha)$ for the throttle angle α = 55°, 60°, 65°, 70°, 75°, 80° and 85°; respectively. Fig. 5(b) shows frequency responses of $E(s, Q_F)$ for steady-state fuel supply rate equals to 169, 203, 239, 276, 321, 384, and 472 *LPH*; respectively. The given fuel supply rates are found by relations given in Fig. 2(a) for different value of α.

Figs. 5(c) and 5(d) show frequency responses of the linearized model N_G/α_c and T_G/α_c shown in Fig. 1 for different value of α. Those frequency responses are derived from those of curves given in Figs.5(a) and 5(b) and frequency responses of the servo system A(s) shown in Fig.1. The frequency responses curves shown in Figs. 5(c) and 5(d) will be used for analyses and designs of the speed control system. They show that the considered system is a large parameter variation system. In general, it needs large loop gain or integration to reduce the effect of parameter variations or steady-state error.

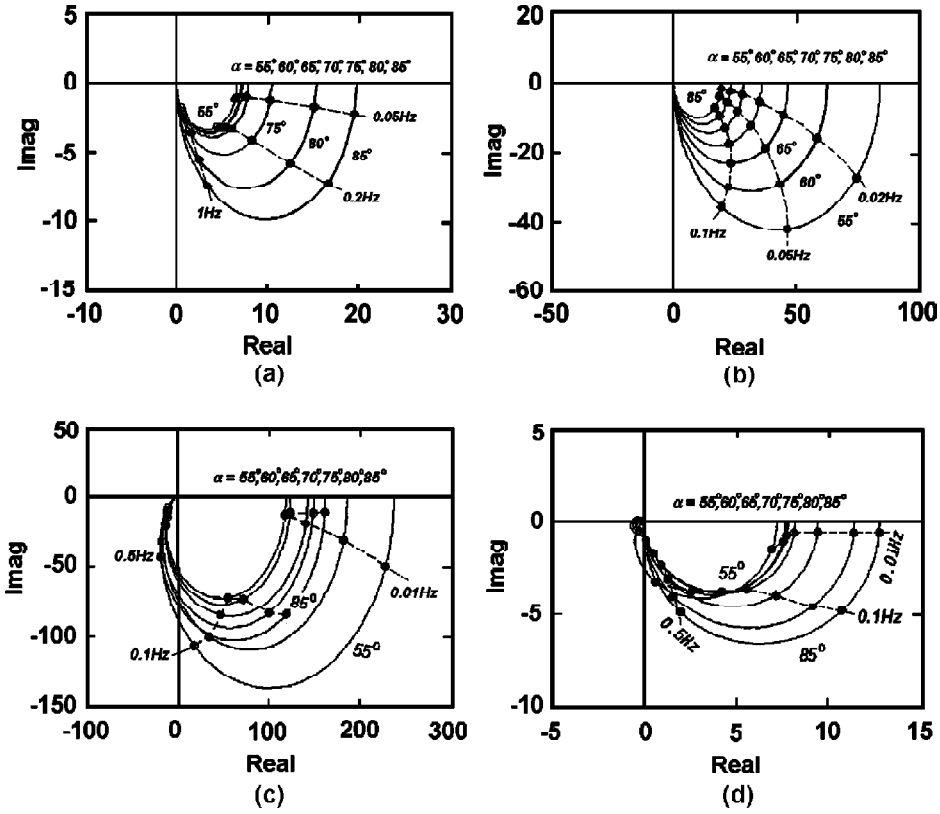

Figure 5: Frequency Responses of (a)$Q(s, \alpha)$, (b) $E(s, \alpha)$, (c)Engine Speed vs. α, (d) Engine Temperature vs. a for α =55°, 60°, 65°, 70°, 75°, 80° and 85°

4. SPEED CONTROL SYSTEM DESIGNS

Now, consider compensations $G_o(s)$ and $G_i(s)$ given Fig. 1. Fig. 6 shows the control structure of the nonlinear speed governor. The integration of the error signal e_o is used for tracking accuracy and intelligent nonlinearities are used to prevent windup of the integrator for throttle angle is limited in α_1. The operation behavior is : if the value of V'_C is greater than that of V_{CS}, then the output value of the integrator Y_S is reset to be $V_{CS} - Y_P$. This is an anti-windup procedure to prevent undesirable overshoot. Fig. 7 shows the command rate limiter. The loop with W_d and 1/s represents derivative loop to find the derivative of the throttle command α_C. The saturating levels P

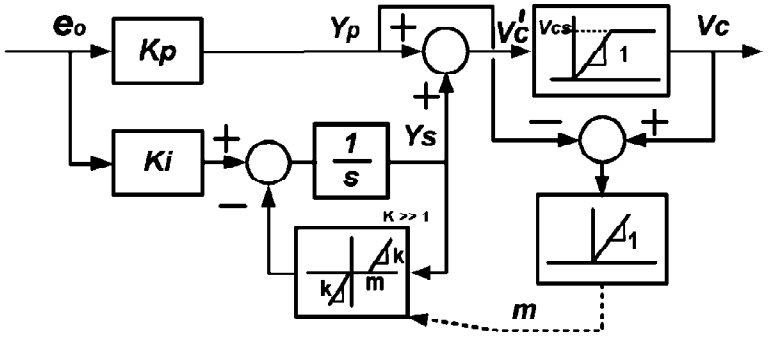

Figure 6: The Intelligent PI Controller G_o(s)

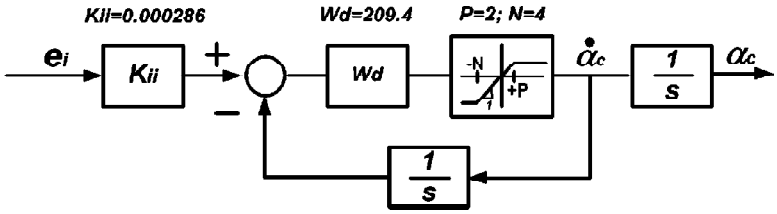

Figure 7: Command Rate Limiter $G_i(s)$

and N represent acceleration and deceleration rate limitations; respectively. The acceleration limit P is used for preventing over-temperature operation. The deceleration N is used for preventing burn-off. Neglecting the nonlinearities of $G_i(s)$ and $G_o(s)$, they are replaced by a constant gain K_{ii} and a conventional PI controller $G_o(s)|_{Linear}$. The suitable value of α_1 can be selected according the desired maximal engine speed and steady-state characteristic curves shown in Fig. 2. In general, the value of α_1 is slightly greater than the found steady-state value of throttle angle with respective to the maximal operating speed.

The considered plant is linearized around steady-state conditions α_{SS}, and all nonlinearities in controllers are first neglected to find desired compensations. Using frequency domain controller design techniques [19], found controllers and low-pass filters are given below:

$$G_o(s)|_{Linear} = k_p + k_i/s = 5 + 2.5/s \tag{16}$$

$$K_{ii} = 2.86 \times 10^{-4} \tag{17}$$

$$H_O(s) = (25s + 75)/(s + 75) \tag{18}$$

$$H_i\,(\mathrm{s}) = 10.73 \tag{19}$$

$$F_O\,(s) = 12.56/(s + 12.56) \tag{20}$$

$$F_i\,(s) = 1.00 \tag{21}$$

The use of $H_o\,(s)$ is to get desired phase margin and frequency fall-off rate for N_G/N_{GC}; simultaneously. It is a two degree of freedom design. Noise filtering is not needed for slow variation of the engine temperature; i.e.; $F_i(s) = 1.00$. The larger value of $H_i(s)$, the better damp and slower bandwidth of the system will be. Suppressing temperature $T_o = 650°\mathrm{C}$ is selected for the considered system. It is less than the steady-state temperature for 35000RPM operation. The found phase margins are greater than 80° with crossover frequencies approaches to be 0.02Hz. The found gain margins are greater than 50dBs. The found bandwidths are about 0.02Hz. It is a good design results comparing to the LQR design (>60deg; > 6dBs).

5. DIGITAL SIMULATIONS AND TEST VERIFICATIONS

Now performing digital simulations of the overall system, the nonlinearities shown in Figs. 6 and 7 are added. The saturation level V_{CS} = 23000 is selected. The value of N = 4 and P = 2 are selected. The cut-off frequency of the derivative loop in $G_i(s)$ is 33.3Hz. The limitations of the throttle angle are selected to be α_0 = 55° and α_1 = 88°. Simulation results with and without the proposed anti-windup controller are shown in Fig. 8 with initial engine starting speed 7000RPM. The speed command N_{GC} is equal to 27300RPM before 30 seconds; equal to 35000RPM between 30 and 50 seconds; and equal to 27300RPM after 50seconds. Figs. 8(a), 8(b), 8(c) and 8(d) show time responses of throttle angle, fuel supply rate, engine speed, engine temperature; respectively. The dash-lines show time responses without anti-windup. The solid-lines show time responses with the proposed anti-windup compensations. The circles shown in Figs. 8(a), 8(c) and 8(d) are real testing datum of the considered system compensated by the proposed nonlinear controllers. From simulation and testing results, one can see that the simulating results give good agreement with the testing datum. This implies that proposed dynamic models and temperature estimator given by Eqs.(4),(5),(8),(10),(15) those illustrated in Fig.3 and Fig.4 provide good description(or modeling) for the turbofan engine.

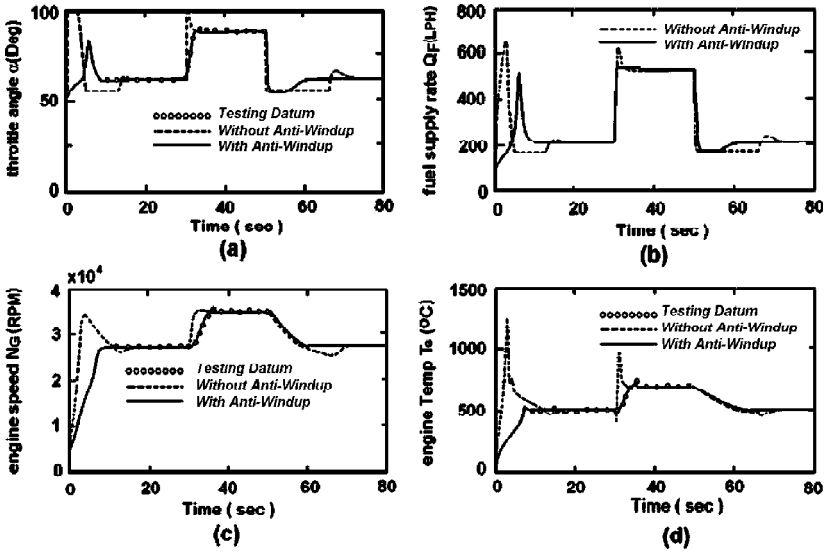

Figure 8: Simulations and Testing Verifications (a) throttle angle vs. time; (b) fuel supply rate vs. time; (c) engine speed vs. time; (d) engine temperature vs. time

Furthermore, it can be seen also that increment of the fuel into engine shown in Fig. 8(c) is limited with the proposed nonlinear controller (solid-line). It can be seen that temperature increments are limited for Q_F is limited by the proposed compensation. Engine temperature exceeds permitted temperature with the conventional PI controller (>1000° *C*). This is due to unexpected fuel flowing rate increment for larger engine speed deviation between command N_{GC} and speed feedback signal N_{GF}. The phase/gain margins of the linear system designs given Section IV are 80deg/50dBs. It is a good design results comparing to the LQR design or other robust design techniques [12-14]. Thus, it can be concluded that nonlinear compensation proposed is better than that of the linear controller.

6. CONCLUSIONS

In this literature, nonlinear dynamic models and a nonlinear speed governor with temperature suppression have been proposed and evaluated for a cruise missile turbofan engine. Low order dynamic models were derived

from measured steady-state datum. Large signal model was used for simulation verification, and small signal model was used for analyses and controller designs. From the real testing and simulation results of the controlled system, one can see that proposed dynamic models give good description for the real system and the nonlinear speed governor makes the controlled system have good performance and less engine temperature increment than that of the linear speed governor.

REFERENCES

[1] G. Brown, Scene matching for navigation updating, *IEE Colloquium* (Digest), pp. 1–3, 1984.

[2] T. Li, Z. Chen, Z. Liu and R. Wang, Estimation of navigation parameters from real-time aerial scene, *Proceedings of SPIE-The International Society for Optical Engineering*, pp. 230–235, 2000.

[3] G. M. Landau, U. Vishkin, Pattern matching in a digitized image, *Algorithmica*, Vol. **12**, No. 4, pp. 375–408, 1994.

[4] O. Taiwo, Design of a multivariable controller for a high-order turbofan engine model by Zakian's method of inequalities, *IEEE Transactions on Automatic Control*, Vol. **23**, No. 5, pp. 926–928, 1978.

[5] S. S. Mahil, S. Bommaraja, A low order optimal controller for a turbo-fan jet engine, 1992 Industry Applications Society Annual Meeting, Vol. **2**, pp. 1717–1720, 1992.

[6] D. C. Hill, Reduced order modeling of gas turbine engines, IEE Colloquium on Identification of Uncertain System, pp.4/1-4/3, 1994.

[7] C. Evans, D. Rees, D. Hill, Frequency-domain identification of gas turbine dynamics, *IEEE Transactions on Control Systems Technology*, Vol. **6**, No. 5, pp. 651–662, 1998.

[8] R. Leibov, Aircraft turbofan engine linear model with uncertain eigenvalues, *IEEE Transactions on Automatic Control*, Vol. **47**, No. 8, pp. 1367–1369, 2002.

[9] W. C. Merrill, Identification of multivariable high-performance turbofan engine dynamics from closed-loop data, J. *Guidance Control & Dynamics*, Vol. **7**, No. 6, pp. 677–683, 1984.

[10] N. V. Kulkarni and K. KrishnaKumar, Intelligent engine control using an adaptive critic, *IEEE Transactions on Control Systems Technology*, Vol. **11**, No. 2, pp. 164–173, 2003.

[11] C. Tournes and Y. B. Shtessel, Controlling transient deviations from adaptation lines in turbojet engine compressor fields via sliding mode, *Proceedings of the IEEE International Conference on Control Applications*, pp. 791–796, 1997.

[12] P. F. Puleston, S. Spurgeon, G. Monsees, Automotive engine speed control: A robust nonlinear control framework, *IEEE Proceedings on Control Theory and Applications*, Vol. **148**, No.1, pp. 81–87, 2001.

[13] B. S. Kwitegetse and M. Kinnaert, Design of LOG/LTR controller: application to a turbofan engine, Proceedings of the 30th *IEEE Conference on Decision and Control*, Vol. **3**, pp. 2826–2827, 1991.

[14] W. C. Merrill, B. Lehtinen and J. Zeller, The role of modern control theory in the design of controls for aircraft turbine engines, *J. Guidance Control & Dynamics*, Vol. **7**, No. 6, pp. 652–661, 1984.

[15] N. Kapoor and A. R. Teel, A dynamic windup compensation scheme applied to a turbofan engine, *Proceedings of the 36th IEEE Conference on Decision and Control*, Vol. **5**, pp. 4689–4694, 1997.

[16] D. K. Frederick, S. Garg and S. Adibhatla, Turbofan engine control design using robust multivariable control technologies, *IEEE Transactions on Control Systems Technology*, Vol. **8**, No. 6, pp. 961–970, 2000.

[17] M. V. Kothare, P. J. Campo, M. Morari and C. N. Nett, A unified framework for the study of an anti-windup designs, *Automatica*, Vol.**30**, pp. 1869–1883, 1994.

[18] A. Visioli, Modified anti-windup scheme for PID controllers, *IEEE Proceedings-Control Theory and Applications*, Vol. **150**, No.1, pp. 49–54, 2003.

[19] B. C. Kuo, Automatic control system, Prentice Hall, New Jersey, 1995.